Journal of Geochemical Exploration 182 (2017) 10–21

Contents lists available at ScienceDirect

Journal of Geochemical Exploration

journal homepage: www.elsevier.com/locate/gexplo

Structures of the Zhazixi Sb–W deposit, South China: Implications for ore genesis and mineral exploration

Guoping Zeng[a], Yongjun Gong[a,*], Zhaofei Wang[b], Xinlu Hu[a], Suofei Xiong[a]

[a] Faculty of Earth Resources, China University of Geosciences, Wuhan 430074, PR China
[b] Anhua Zhazixi Antimony Mining Co. Ltd., Anhua, Yiyang 413507, PR China

ARTICLE INFO

Keywords:
Xuefeng uplift belt
Zhazixi Sb–W deposit
Structures
Ore genesis
Mineral exploration

ABSTRACT

The Zhazixi Sb–W deposit is located in the Xuefeng uplift belt, South China. It is a structurally controlled hydrothermal vein-type deposit with unique metal associations of Sb and W. Field investigations suggest that structures in the Zhazixi Sb–W deposit are dominated by NW-trending faults and interlayer fractures. The former are critical to Sb mineralization, which is simplified by quartz-stibnite veins. In contrast, the latter are closely associated with W mineralization, which is predominantly composed of quartz-scheelite veins. Kinematic analyses suggest that the NW-trending faults experienced a sinistrally transpressional tectonic movement before Sb mineralization and converted to an extensional kinematic regime during Sb mineralization. Rose diagrams and stereographic projection of W-bearing fractures indicate that the interlayer fractures may form under compressional stress in a NW–SE direction. Ore genesis is discussed based on the geological and geochemical features, which indicate the metal associations of Sb and W are a superposition of two separate ore-forming periods that took place during the early Mesozoic intracontinental orogeny. Finally, integrated with the trend surface of Sb, the ore grade distribution regularities are discussed and favorable mineral exploration areas of Sb and W are proposed in the Zhazixi Sb–W deposit.

1. Introduction

Most antimoniferous deposits in the world are characterized by monomineralic Sb (Dill, 1985; Wu, 1993; Fan et al., 2004a), Au–Sb (Dill et al., 1995, 1997; Hagemann and Lüders, 2003; Zaw et al., 2007; Neiva et al., 2008; Yang et al., 2009; Brogi and Fulignati, 2012) or sulfphantimonates-base metal deposits (Wagner and Cook, 1998, 2000), which are famous for the Dachang deposit in South China (Wu, 1993; Fan et al., 2004b). Many antimoniferous deposits featuring metal assemblages of Sb and W are also important Sb reserves in the world (Arribas and Gumiel, 1984; Afanas'eva et al., 1994; Akçay, 1994), especially in South China (Wu, 1993; Yang and Blum, 1999). The geology, mineralogy, geochemistry, and ore-forming fluids of the Sb–W ± (Au) deposits in South China have been extensively studied (Peng et al., 2003; Peng and Frei, 2004). However, these studies focused on Sb, ignoring the relationship between Sb and W mineralization, and argued that Sb and W to precipitate in a single metallogenic process (Murao et al., 1999; Gu et al., 2007, 2012), despite the fact that most Sb formed in epithermal hydrothermal fluids (Williams-Jones and Norman, 1997; Hinsberg et al., 2003), whereas mass of W deposited moderate-high temperature hydrothermal systems (Robb, 2004; Dill et al., 2008).

The Xuefeng uplift belt in South China contains a large number of Sb–W ± (Au) deposits, including the Zengjiaxi, Zhazixi (Peng et al., 2008, 2010), and Woxi (Peng and Frei, 2004; Zhu and Peng, 2015). The Zhazixi Sb–W deposit in the Xuefeng uplift belt is marked by Sb mineralization of its lode and for large strata-bounded W mineralization, and consists of 25×10^4 t Sb with an average grade of 9.46% and 1.3×10^4 t WO_3 with an average grade of 0.824%. The Zhazixi Sb–W deposit provides a rare opportunity for studying the Sb–W ± (Au) deposits in the Xuefeng uplift belt.

In this paper, the structures and grade distribution regularities of Sb and W of the Zhazixi Sb–W deposit are presented to highlight the difference between Sb and W mineralization and discuss the ore genesis of the Sb–W ± (Au) deposits in the Xuefeng uplift belt and evaluate exploring targets both in the Xuefeng uplift belt and the Zhazixi Sb–W deposit.

* Corresponding author at: 388, Lumo Road, Hongshan District, China University of Geosciences, 430074 Wuhan, PR China.
E-mail address: gyjxhz@163.com (Y. Gong).

http://dx.doi.org/10.1016/j.gexplo.2017.07.010
Received 6 May 2016; Received in revised form 23 June 2017; Accepted 15 July 2017
Available online 20 July 2017
0375-6742/

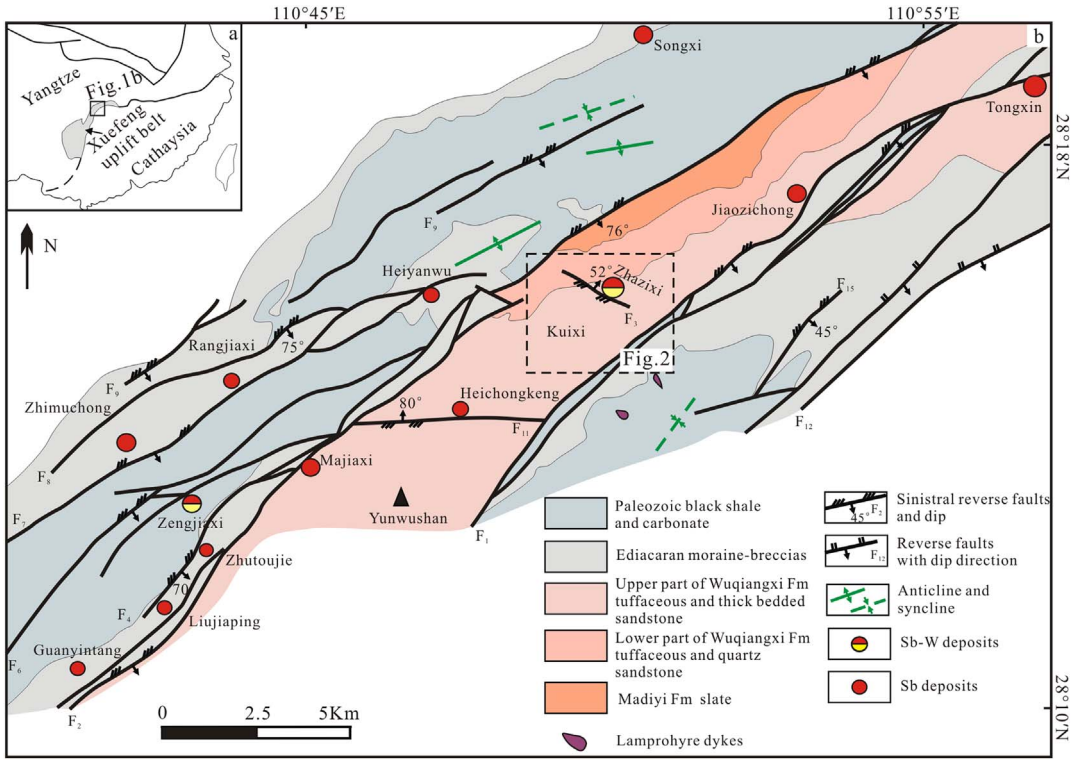

Fig. 1. (a) Tectonic outline of South China displaying the location of the Xuefeng uplift belt and the study area (Modified after Zhai, 2013); (b) geological sketch of Zhazixi Sb ore belt showing the location of the Zhazixi Sb–W deposit (Modified after HBGMR, 2010).

2. Regional geological setting

2.1. Xuefeng uplift belt

The Xuefeng uplift belt is an orogenic belt with numerous antimoniferous deposits between the Yangtze and Cathaysia blocks in South China. The Xuefeng uplift belt trends to the northeast in its southwestern part and reorients to the east in its northeastern part (Fig. 1a) (HBGMR, 1988). Evidences regarding magmatism, structures, metamorphic deformation and paleomagnetism suggest that the Xuefeng uplift belt experienced multiphase tectonic movements (Otofuji et al., 1998; Chen et al., 2001; Shu, 2012; Liu et al., 2013). The Xuefeng uplift belt occurred as an active continental margin in the Mesoproterozoic and featured by deepwater turbidite rocks. The Grenville Orogeny between ~1000 and ~800 Ma generated many NE- and EW-trending deep fractures and deformed the Meso-Neoproterozoic rocks extensively and metamorphosed them into sub-greenschist facies (Qiu et al., 2000; Wu et al., 2006; Li et al., 2008; Li et al., 2009; Bai et al., 2011; Zhai, 2013; Yao et al., 2014). During the breakup of the Rodinian supercontinent, sedimentary rocks of the continental slope facies of the passive continental margin dominated the Xuefeng uplift belt. The intracontinental orogeny in the early Paleozoic and Mesozoic generated compressional stress in the NW–SE direction and reactivated preexisting faults (Ren, 1990; Qiu et al., 1998; Liang et al., 1999; Shu, 2006; Shu et al., 2008; Li and Li, 2007).

The Meso-Neoproterozoic clastic rocks of the sub-greenschist facies in the Xuefeng uplift belt shows weak enrichment of Sb and W, with Sb and W concentrations 4.7–7.0 and 1.5–1.7 times higher than their crustal averages (He et al., 1996; Lu et al., 2001; Ma et al., 2002).

2.2. Zhazixi Sb ore belt

The Zhazixi Sb ore belt containing the Zhazixi Sb–W deposit is located in the central part of the Xuefeng uplift belt. The rocks were dominantly formed in the Neoproterozoic to Paleozoic (Fig. 1b). The Neoproterozoic Madiyi and Wuqiangxi Formations are the oldest lithologic units exposed in the belt. The Madiyi Formation features green and red low-grade metamorphic slate. The Wuqiangxi Formation is composed of sub-greenschist facies metamorphic detrital and pyroclastic rocks and can be subdivided into two lithologic parts. The Ediacaran moraine-breccia and Paleozoic black shale and carbonate cover the Wuqiangxi Formation discordantly. The Zhazixi ore belt is constrained by regional NE-trending F_1 and F_2 faults, which strike to the NE-NNE and dip to the SE (Fig. 1b). The fault zones are filled by wall rock lenses, and mylonite with widespread silicification and sericitization. Sb-bearing veins can be found locally. The scratching on fault surfaces and stratigraphic relationship of the opposite sides suggest a sinistrally transpressional property, with the hanging wall obliquely thrust to the NE (HBGMR, 2010). Secondary NE-, NW-, and EW-trending faults are common in this belt, whereas the NE-trending folds are insignificant in the rocks from the Ediacaran to Paleozoic (Fig. 1b). Intrusive rocks are scarce in the Zhazixi ore belt, occurring as lamprophyre dykes in the hanging wall of the F_1 fault (HBGMR, 2010).

Antimoniferous deposits are widespread throughout the Zhazixi Sb ore belt. Mineralization usually occurs in the Proterozoic sub-greenschist facies clastic rocks, and presents elemental associations of Sb ± W (Hu et al., 2007), such as the Zengjiaxi Sb–W deposit, the Zhazixi Sb–W deposit (Wang et al., 2012), and the Tongxin Sb deposits (Fig. 1b). The Sm–Nd isochron age of scheelite (227.3 ± 6.2 Ma, Wang et al., 2012) has been interpreted to be the mineralization age of W.

3. Deposit geology

Sedimentary rocks in the Zhazixi Sb–W deposit consist mainly of the Neoproterozoic Wuqiangxi Formation, with Ediacaran moraine-breccia and Cambrian black shale discordantly covering the Wuqiangxi Formation. The Wuqiangxi Formation is composed of sub-greenschist facies metamorphic detrital rocks and pyroclastic rocks striking to the NE and dipping to the SE with dip angles ranging from 41 to 48° (Fig. 2). The lower part is composed of tuff, tuffaceous sandstone, and

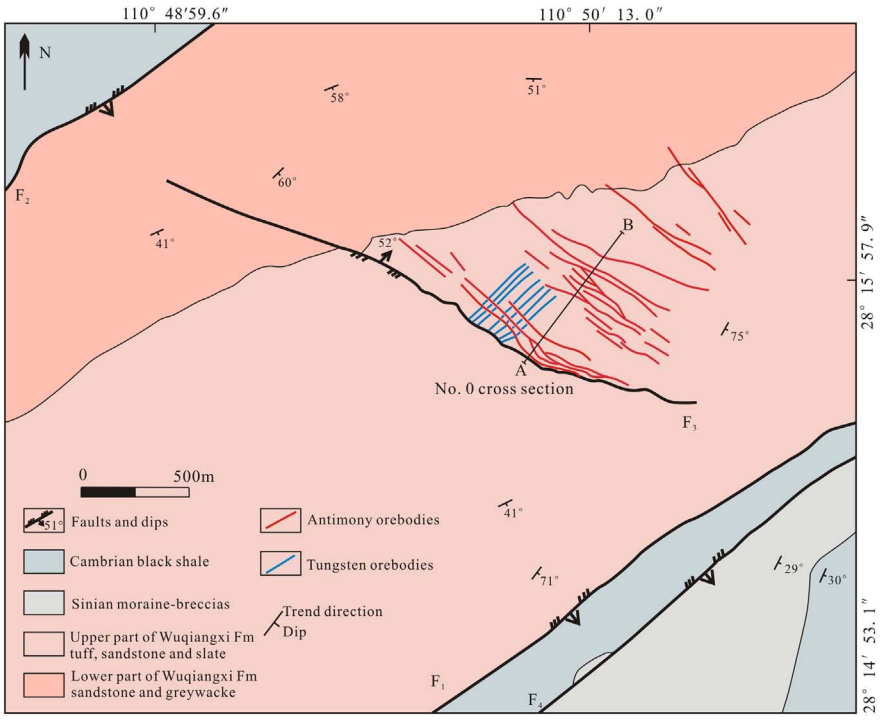

Fig. 2. Geological map of the Zhazixi Sb–W ore deposit (Modified after HBGMR, 2010).

quartz sandstone. The upper part is dominated by thick-bedded sandstone, tuffaceous sandstone, and greywacke and acts as primary wall rocks for W orebodies in the Zhazixi Sb–W deposit.

Structures in the Zhazixi Sb–W deposit are dominated by NW-trending faults and interlayer fractures (Fig. 2). The former are simplified by the NW-trending F_3 fault and its secondary faults on the hanging wall. The latter are composed of the interlayer sliding interfaces between tuffaceous sandstone and thick-bedded sandstone, with its secondary tiny fractures in the thick-bedded sandstone. The interlayer fractures are evidently crosscut by the NW-trending faults, suggesting the interlayer fractures predate the NW-trending faults (Figs. 2, 3).

In the Zhazixi Sb–W ore deposit, Sb orebodies, primarily hosted by the NW-trending faults, consist of quartz-stibnite veins (Fig. 4a); whereas W orebodies within the interlayer fractures are predominantly composed of quartz-scheelite veins (Fig. 4b). The W orebodies are offset by the Sb orebodies (Fig. 4c).

The Sb orebodies strike 290–330° NWW and dip 55–88° NE–NNE in the Zhazixi Sb–W deposit (Figs. 2, 3). The No.1 Sb orebody is representative in the ore district. It is 80–235 m along the strike, 818 m along the plunge and is 0.12–2.96 m thick. The Sb grade spans from 0.25% to 44.27%, with an average of 11.07%. The Sb mineralized zones are dominated by stibnite (Fig. 4e), with a small amount of native Sb, berthierite, chalcostibnite, pyrite, and chalcopyrite (Fig. 4d–g). The gangue minerals primarily contain quartz and minor rutiles. The hydrothermal alteration is characterized by silicification, with trace amounts of sulfidation.

The W orebodies are mainly lenses and are usually parallel to the wall rocks, striking 20–58° NE and dipping 57–69° SE (Figs. 2, 3). The W orebodies are generally 30–200 m long along strike and 320 m along plunge. Scheelite is the only ore mineral within W mineralization (Fig. 4e). Gangue minerals include massive quartz, minor chlorite, and calcite. The hydrothermal alteration is characterized by intensive silicification, with minor chloritization and carbonatization (Fig. 4e–g).

4. Samples and methods

In order to address the structural and mineralization characteristics, geologic mapping and microscopic investigations were performed. The strikes and dips of faults, fractures and orebodies in the Zhazixi Sb–W deposit were also measured with a magnetic compass.

Stereographic projections of ore veins were plotted with AutoCAD software. Rose diagrams of tiny W-bearing fractures were plotted with Stereonett software. Stereographic projections and rose diagrams were selected to analyze the kinematic features of the structures in the Zhazixi Sb–W deposit.

The trend surface of Sb grades was plotted to study the Sb distribution rules of the Zhazixi Sb–W deposit. A total of 197 ore samples with corresponding coordinates (x = geodetic coordinates; y = elevation) were collected on the No.0 cross section and analyzed for Sb concentrations (wt%). The sampling data were of sufficient quantity and uniformly distributed to fit the Sb grade distribution.

Representative samples from underground exposures of the Zhazixi Sb–W deposit were collected for hydrogen and oxygen isotopic analyses. Quartz grains were separated by careful handpicking under a binocular microscope. Hydrogen and oxygen isotopic compositions of quartz were measured with using a MAT-251 mass spectrometer at the Deposit Geology Institute, Chinese Academy of Geological Sciences, Beijing Wang et al. (2013). The δD_{H2O} values were measured from fluid inclusions with an analytical precision of ± 2‰. The $\delta^{18}O_{H2O}$ values were calculated from $\delta^{18}O_{quartz}$ values with an analytical precision of ± 0.2‰ using the formula: $1000\ln\alpha_{quartz-water} = 3.38 \times 10^6/T^2 - 3.40$ (Clayton et al., 1972), regarding homogenization temperatures of fluid inclusions in quartz.

5. Results

The NW-trending faults and the interlayer fractures were evaluated separately in the Zhazixi Sb–W deposit.

5.1. NW-trending faults

According to their scale and their contributions to the Sb mineralization, three orders of NW-trending faults can be identified in the Zhazixi Sb–W deposit. The NW-trending F_3 fault is the first order and also the most important Sb-controlling structure (Fig. 2). The 20.7-m-

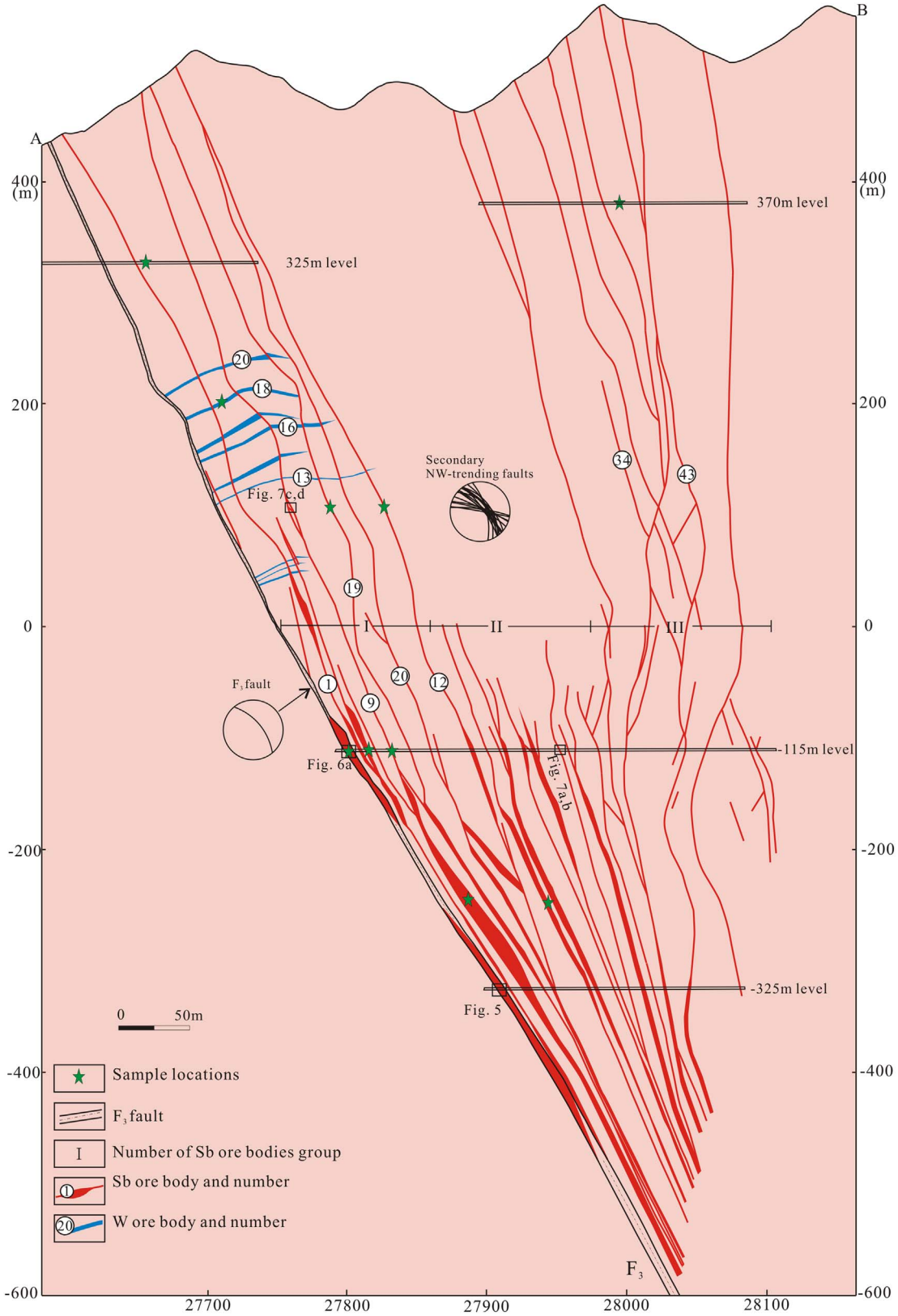

Fig. 3. No. 0 cross section showing the structure patterns and minerlization styles of the Zhazixi Sb–W deposit (Modified after HBGMR, 2010).

wide F_3 fault extends approximately 2.6 km along a strike of 295° and dips to the NE at angles of 52–80°. The fault surface is gently wavy with a gentle dip in the upper part and steep dip in the lower part. Sinistrally movement with 80 m horizontal and vertical displacements present in the F_3 fault. Stibnite is detected in the deep part of the F_3 fault, indicating the F_3 fault acts as a pathway for Sb-bearing fluids (Fig. 3). The F_3 fault can easily be subdivided into three structural zones from bottom to top. The first structural zone is primarily characterized by sandstone lenses, which contain acicular stibnite and are partitioned by network of cracks (Fig. 5a, c, d). The second structural zone in the

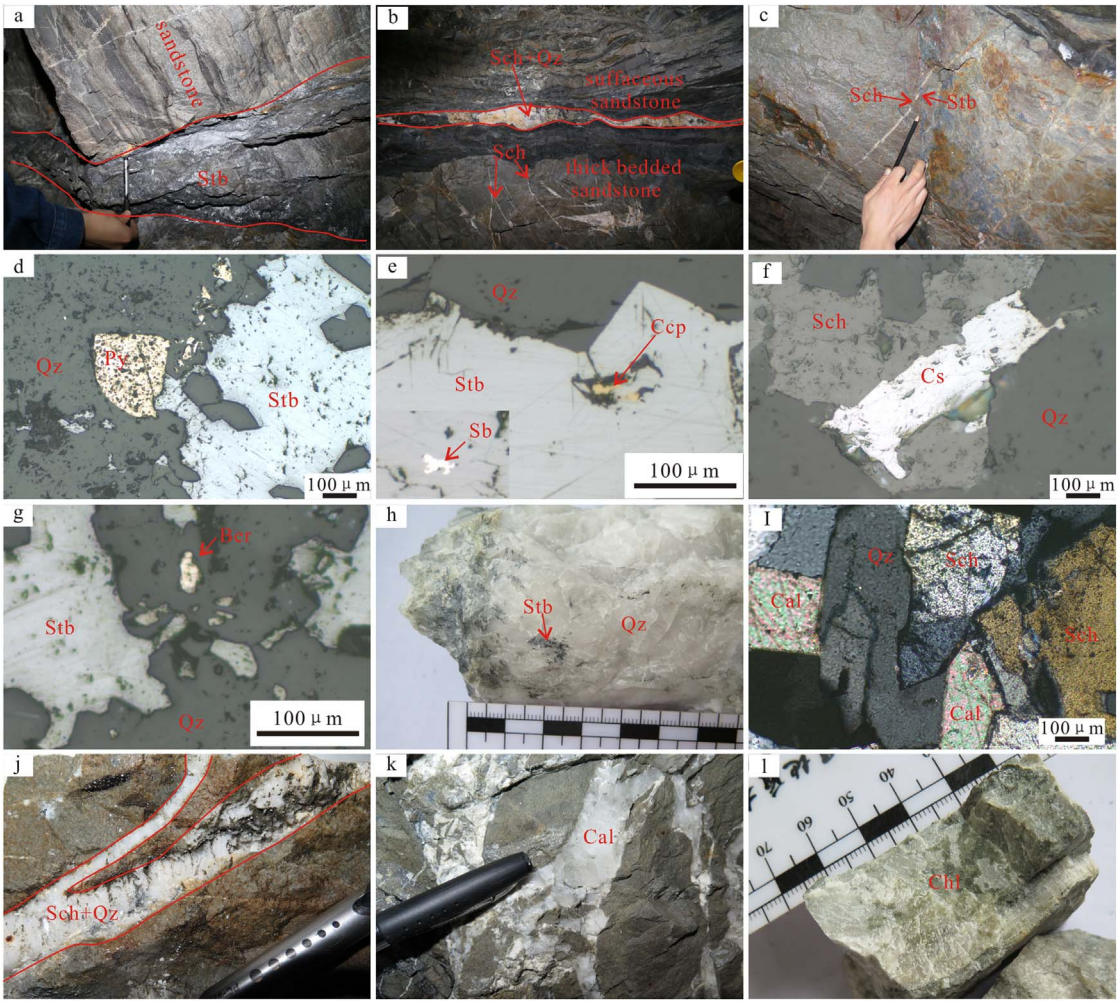

Fig. 4. Representative photographs showing the mineralization features of the Zhazixi Sb–W ore deposit. (a) Quartz-stibnite veins crosscut the sandstone; (b) Quartz-scheelite veins in the slip interfaces and thick-bedded sandstone; (c) Quartz-stibnite vein crosscut quartz-scheelite vein; (d) Sulfidation. Disseminated pyrite coexisting stibnite and quartz (under microscope); (e) Chalcopyrite and native antimony replaced by stibnite (under microscope); (f) Chalcostibnite occurs as lath shaped and appears to replace scheelite (under microscope); (g) Berthierite appears as isolated grains in the quartz aggregates; (h) Silification, acicular stibnite in quartz vein; (I) Coarse-grained, euhedral and subhedral calcite coexisting with scheelite and quartz (under microscope); (j) Silification, quartz-scheelite veins in the sandstone; (k) Carbonation, calcite vein in sandstone; (l) Chloritization, chlorite in the quartz-scheelite vein.
Mineral abbreviations: Stb = stibnite, Sch = scheelite, Qz = quartz, Py = pyrite, Ccp = chalcopyrite, Sb = native antimony, Cs = chalcostibnite, Ber = berthierite, Cal = calcite; Ch = Chlorite.

center of the F_3 fault consists of a black argillaceous schistosity zone and Sb free quartz lenses. The long axes of quartz lenses are parallel to the argillaceous schistosity zone, suggesting it is synchronous with tectonic activity (Fig. 5a, b). The third structural zone includes a wide range of lenticular wall rock partitioned by network fractures with oxidized gouge. The complex fabric features of the F_3 fault imply a multiphase tectonic movement evolution.

In the F_3 fault, the intensively argillaceous schistosity zone may have formed before the Sb mineralization. Some secondary transpressional fractures also developed in the underside wall rock (Fig. 6a). A stereographic projection with the strikes and dips of the argillaceous schistosity zone and its secondary transpressional faults was plotted with AutoCAD software to illustrate a sinistrally compressional property of the pre-mineralization tectonic activity (Fig. 6b).

The secondary faults on the hanging wall of the F_3 fault are dominated by NW-trending faults, with minor NE- and EW-trending faults. The secondary NW-trending faults strike to the NW 290–330°, and dip to the NNE–NE with angles generally greater than 60° and converge with the F_3 fault in the deep part. In terms of mineralization, these secondary NW-trending faults are the most important Sb-bearing structures in Zhazixi Sb–W deposit (Fig. 3).

The secondary Sb-bearing faults swell, branch and converge locally (Fig. 7a, b). For instance, the No. 9 Sb vein is hosted in a fault zone constrained by two compressive structural planes (Fig. 7c). The wall rocks in the fault zone are deformed into structural lenses (Fig. 7c), then are transformed into breccias and cemented by Sb-bearing network veins (Fig. 7d). In addition, wall rock breccias, with varying sizes and irregular shapes, are also evident in the Sb-bearing veins (Fig. 7e, f). The structural lenses in the fault zones reflect a transpressional movement prior to Sb mineralization, whereas the breccias are cemented by Sb-bearing network veins, indicating an extensional kinematic regime during Sb mineralization.

The third faults are dominated by a great number of tiny tensional and shear fractures bearing stibnite in sandstones adjacent to the secondary NW-trending faults. The combination of tensional and shear fractures suggests extensional normal faulting (Fig. 8a). Sb-bearing stockwork were evidently developed at the intersection of tensional fractures (Fig. 8b). This study proposes that the third faults also developed under an extensional kinematic regime, which was coincident with the secondary NW-trending faults during Sb mineralization.

According to the kinematic analyses, we propose that the NW-trending faults of three orders in the Zhazixi Sb–W deposit are consistent in the kinematic regime and shared a synchronous tectonic evolution, experiencing a sinistrally transpressional tectonic movement

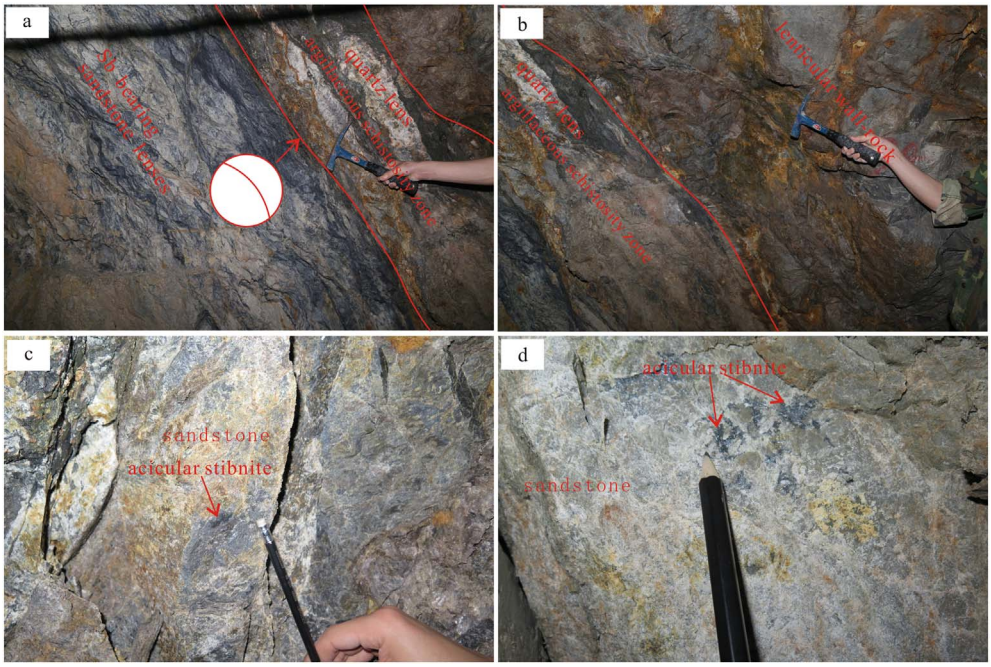

Fig. 5. Field photographs showing the features of the F_3 fault. (a) The first and second structural zones of the F_3 fault; (b) The second and third structural zones of the F_3 fault; (c) and (d) Acicular stibnite-bearing sandstone of the first structural zone.

before Sb mineralization, and then displayed as an extensional kinematic regime during Sb metallogenic period.

5.2. Interlayer fractures

The interlayer fractures are primarily located within the upper part of the Wuqiangxi Formation and are the major W-hosting structures in the Zhazixi Sb–W deposit (Fig. 9). The interlayer fractures consist of sliding interfaces and tiny fractures. The sliding interfaces developed between tuffaceous sandstone and thick-bedded sandstone (Fig. 10a, b). The formation mechanism of the sliding interfaces may be related to the mechanical difference between tuffaceous sandstone and thick-bedded sandstone.

The sliding interfaces enlarge locally, suggesting a dextral movement and performing favorable space for the deposition of quartz and scheelite during W mineralization. The tiny fractures developed in the thick-bedded sandstone also act as important W-bearing structures (Fig. 10c, d).

The tiny fractures are composed of shear and tensional fractures. Shear fractures exhibit en-echelon arrangement in the thick-bedded sandstone, indicating a shear stress (Fig. 11a). Tensional fractures intersect obliquely with the lithologic interface at high angles, showing a linkage to the sliding of the lithologic interface (Fig. 11b). Angular breccia is also enveloped in the tensional fractures in the thick-bedded sandstone (Fig. 11c, d), suggesting a tensional kinematic regime during the W mineralization. Overall, the tiny fractures in the thick-bedded sandstone are genetically related to the shear stress produced by sliding along the lithologic interfaces.

A total of 61 shear W-bearing fractures' and 15 tensional stibnite-bearing fractures' strikes and dips were collected to study the kinematic stress, which generated the interlayer fractures. Rose diagrams of the shear scheelite-bearing fractures are plotted with the Stereonett software. Three groups of dipping can be picked out on the rose diagram, including the approximately 50°, 30° in the northeast, and 240° in the southwest (Fig. 12a). The strikes and dips of these shear scheelite-bearing fractures indicate that the latter two groups are conjugate joints and can be used to determine the directions of three principal stresses with a stereographic projection by using AutoCAD software (Fig. 12b). The maximum principal stress (σ_1) on the stereographic projection strikes at 145° and dips at 71°. Rose diagram of tensional scheelite-bearing fractures made by Stereonett software show the dominant strike direction ranging from 130 to 140° (Fig. 12c). Obviously, the strike direction of the maximum principal stress (σ_1) on the stereographic projection is roughly consistent with that on the rose diagram. The kinematic analyses suggest that the interlayer fractures formed under the regional compressional folding process in the NW–SE direction.

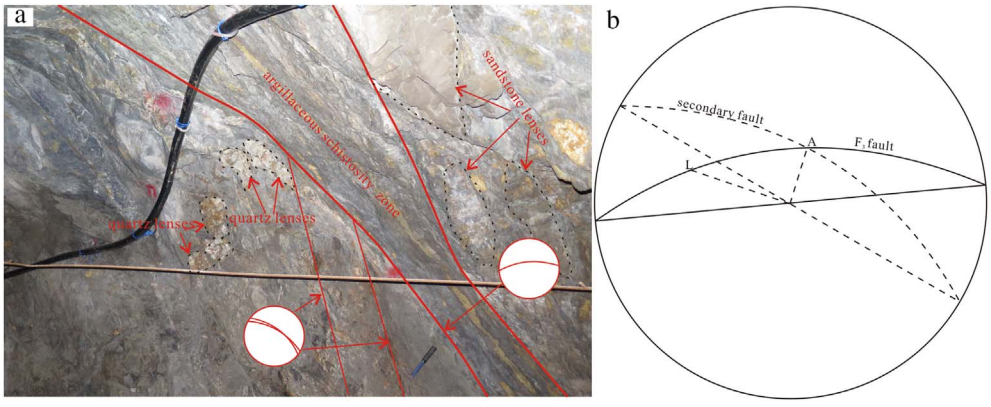

Fig. 6. (a) Field photograph showing the characteristic of the F_3 fault; (b) Stereographic map of fault F_3 and its secondary fault, and point A stands for attitude of intersection line of the two structure planes, point L shows a movement direction of the sinistrally transpressional movement.

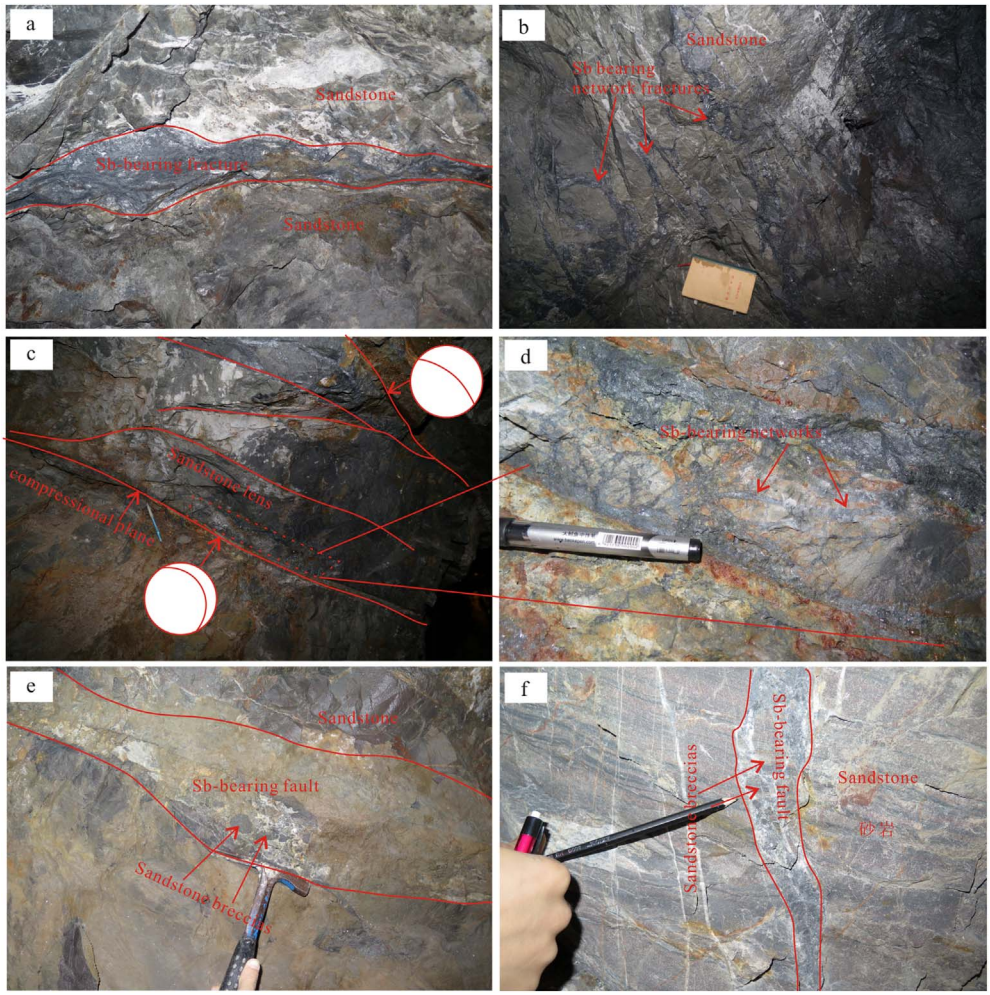

Fig. 7. Field photographs showing the features of secondary Sb-bearing faults. (a) Local enlargement of Sb-bearing faults; (b) Tiny branches of Sb-bearing fractures; (c) Sandstone lenses are located between two transpressional structural planes; (d) Network Sb-bearing fractures; (e) Sandstone breccias in Sb-bearing faults; (f) Sandstone breccias cemented by Sb-bearing fault.

5.3. The trend surface of the Sb grade

A trend surface is an effective way to present the spatial distribution rules of geological variables, and has been widely applied to structural studies, geochemical anomaly separation, and mineral exploration evaluation (Cao and Lu, 2015; Wang and Zuo, 2015).

A pretreatment on the logarithm of the Sb grades indicated that a quadratic trend surface map provides the best fit for the Sb grade surface. The Sb contour and quadratic trend surface diagrams were plotted with the Surfer software. On the Sb contour diagram (Fig. 13a), two groups of linear Sb ore-shoots can be recognized on the hanging wall of the F_3 fault. One group of ore-shoots is adjacent to the F_3 fault and intersects with the F_3 fault in a gentle angle. In contrast, the other group of ore-shoots keeps relatively away from the F_3 fault in the shallow part and intersects with the F_3 fault in a relatively large angle in the deep seated portion. The trend surface of Sb presents an obliquely outspread ellipse (Fig. 13b) and the positive anomaly features highly dense Sb veins.

5.4. Oxygen- and hydrogen-isotopes

The δD_{H2O} values of the quartz–scheelite veins ranged from −86‰ to −66‰ with an average of −74‰. The δD_{H2O} values of quartz-stibnite veins are −96‰ to −74‰ with an average of −83‰. The quartz–scheelite veins and quartz–stibnite veins had $\delta^{18}O_{H2O}$ values varying from 3.95 to 7.8‰ (average of 5.3‰) and 1.8‰ to 7.2‰ (average of 6.0‰), respectively (Table 1).

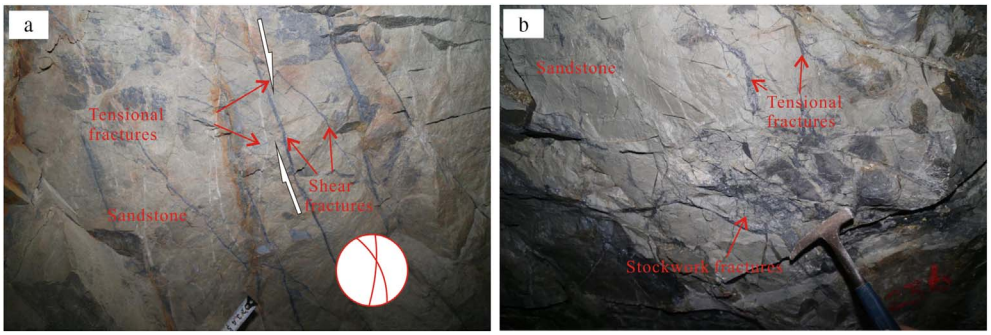

Fig. 8. (a) Intergrowth of shear and tensional Sb-bearing fractures; (b) Tensional Sb-bearing fractures and Sb-bearing stockwork.

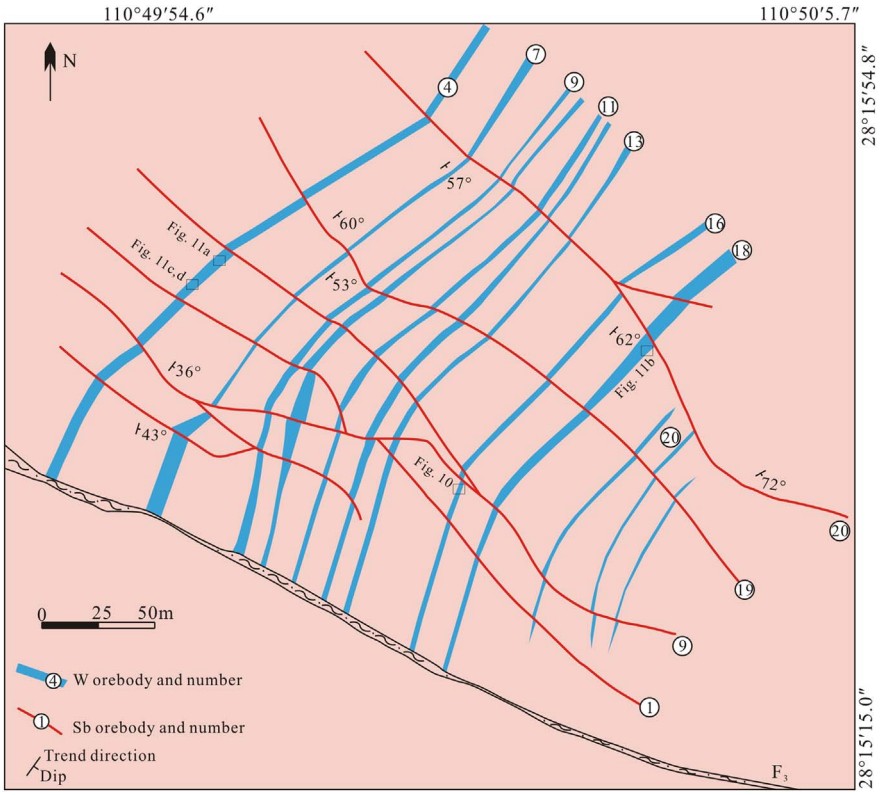

Fig. 9. Geological plane of 325 m level showing the distribution of W-bearing interlayer fractures in Zhazixi Sb–W deposit (Modified after HBGMR, 2010).

6. Discussion

6.1. Ore grade distribution regularities

In the Zhazixi ore belt, most Sb ± W deposits are distributed adjacent to the intersections of the regional NE-trending faults and their secondary NW- and NWW-trending faults (Fig. 1b).

In terms of the Zhazixi Sb–W deposit, the Sb orebodies are primarily concentrated below the elevation of 0 m, whereas the W orebodies are dense above the 325 m level. Between the elevation ranges from 0 to 325 m, the concentration of Sb and W are both relatively weak (Fig. 3).

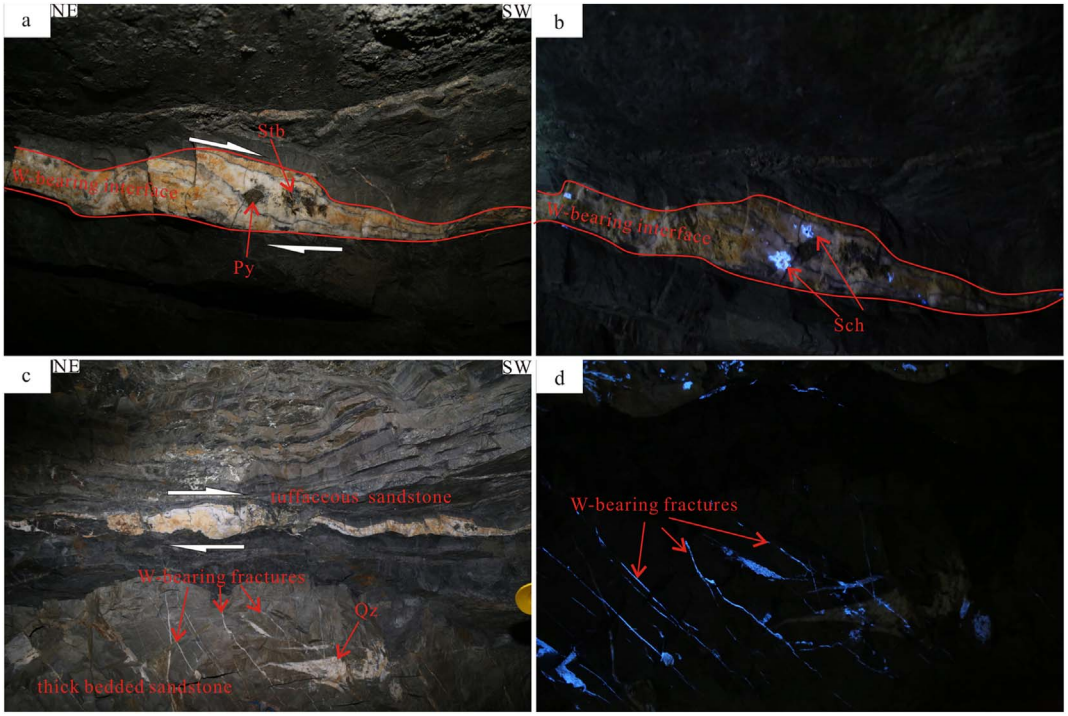

Fig. 10. (a) Scheelite-bearing interlayer sliding interface (normal light); (b) Scheelite-bearing interlayer sliding interface (fluorescence light); (c) Scheelite-bearing tiny fractures in thick-bedded sandstone (normal light); (d) Scheelite-bearing tiny fractures in thick-bedded sandstone (fluorescence light).

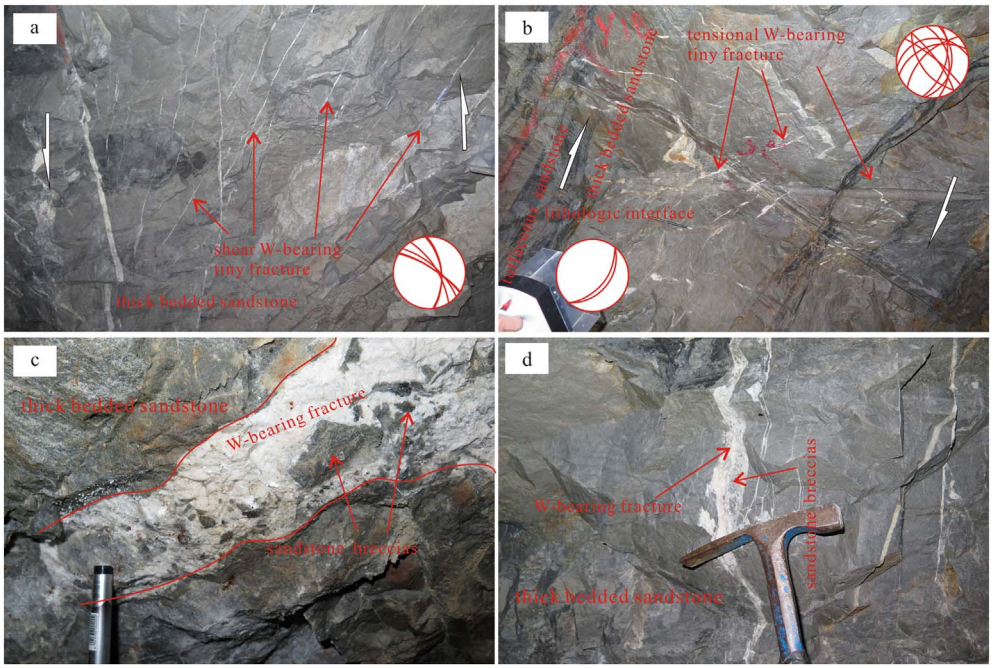

Fig. 11. Scheelite-bearing fractures in the Zhazixi Sb–W deposit. (a) Scheelite-bearing echelon shear fractures; (b) Scheelite-bearing tensional fractures in thick-bedded sandstone; (c) Sandstone breccias enveloped in scheelite-bearing tensional fracture; (d) Sandstone breccias in scheelite-bearing tensional fracture.

6.1.1. Sb distribution regularities

The structural analyses suggest that the Sb distribution is controlled by three orders of NW-trending faults in the Zhazixi Sb–W deposit. Almost all Sb orebodies are located in the hanging wall of the NW-trending F_3 fault, and the overall distribution pattern of Sb orebodies is controlled by the F_3 fault. The kinematic analyses show that the F_3 fault experienced an extensional regime, creating a conduit for the Sb-bearing fluids during Sb mineralization.

The secondary NW-trending faults on the hanging wall are the key hosting structures of Sb orebodies and control the distribution of Sb orebodies directly. The Sb mineralization exhibits reversed horse-tail structures and three groups of Sb orebodiess (I, II, and III) can be recognized in the representative cross section (Fig. 3). Whereas the Sb orebodies are sparse, thin, and widely spaced in the shallow part, they are dense, thick, and narrowly spaced in the deep part. The Sb orebodies all converge toward the deep seated portion of the F_3 fault. Lateral Sb orebodies are also arranged regularly and are intense near the F_3 fault and become weaker away from the fault (Fig. 3).

The tiny shear and tensional fractures in the thick-bedded sandstone are the lowest order of Sb-hosting structures. The tiny Sb ore-veins hosted in the tiny fractures can be of significant economic value when they are dense enough.

The anomalous ore-shoots of Sb in the representative cross section are roughly equidistant and converge in the deep part of the F_3 fault and deeply extend along the F_3 fault. The trend surface of Sb tends to wedge out above an elevation of 0 m with poor Sb grade and shows a downward outspread trend along the F_3 fault, suggesting the Sb-bearing fluids migrate from deep seated portion to shallow space along the F_3 fault.

6.1.2. W distribution regularities

The distribution regularities of W are completely different from those of Sb in the Zhazixi Sb–W deposit. The thick-bedded sandstone can usually be regarded as W stratiform orebody when the tiny scheelite-bearing veins are dense enough, and are similar to the scheelite ore-veins hosted in the sliding interfaces. Thus, the W mineralization in Zhazixi Sb–W deposit is stratabound and jointly controlled by lithology and interlayer fractures in the upper part of Wuqiangxi Formation. Since the development of the interlayer fractures was closely related to the mechanical difference between tuffaceous sandstone and thick-bedded sandstone, the interphase distribution of tuffaceous sandstone and thick-bedded sandstone is critical to W distribution.

No W mineralization is detected in the F_3 fault (Peng et al., 2008, 2010; Wang et al., 2012), indicating that the NW-trending F_3 fault is inactive for the W-bearing fluids migration during W mineralization. Further, the W ore-layers are directly offset by the NW-trending faults (Fig. 9), suggesting that the NW-trending faults activated after W mineralization and displaced the W orebodies.

6.2. Implications for ore genesis

The Sb and W mineralization in the Zhazixi deposit are controlled by different structures and present different mineralization features. The elemental associations of Sb and W are produced by superposition of Sb and W mineralization and took place in two separate periods.

Integrated with the Sm-Nd isochron age of the scheelite, the kinematic analyses suggest that structures in the Zhazixi Sb–W deposit formed during the early Mesozoic intracontinental orogeny. During the orogenic process, the regional compressional stress in the NW–SE

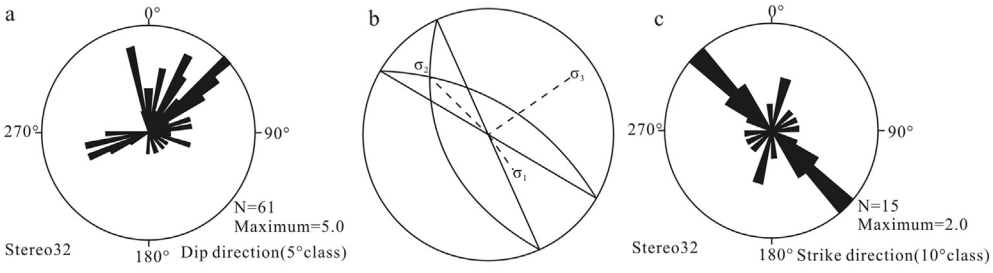

Fig. 12. Diagrams of scheelite-bearing fractures. (a) Rose diagram of shear scheelite-bearing fractures; (b) Stereographic projection of conjugation shear scheelite-bearing fractures, point 1 stands for the direction of σ_1; (c) Rose diagram of tensional scheelite-bearing fractures. (For interpretation of the references to colour in this figure legend, the reader is referred to the web version of this article.)

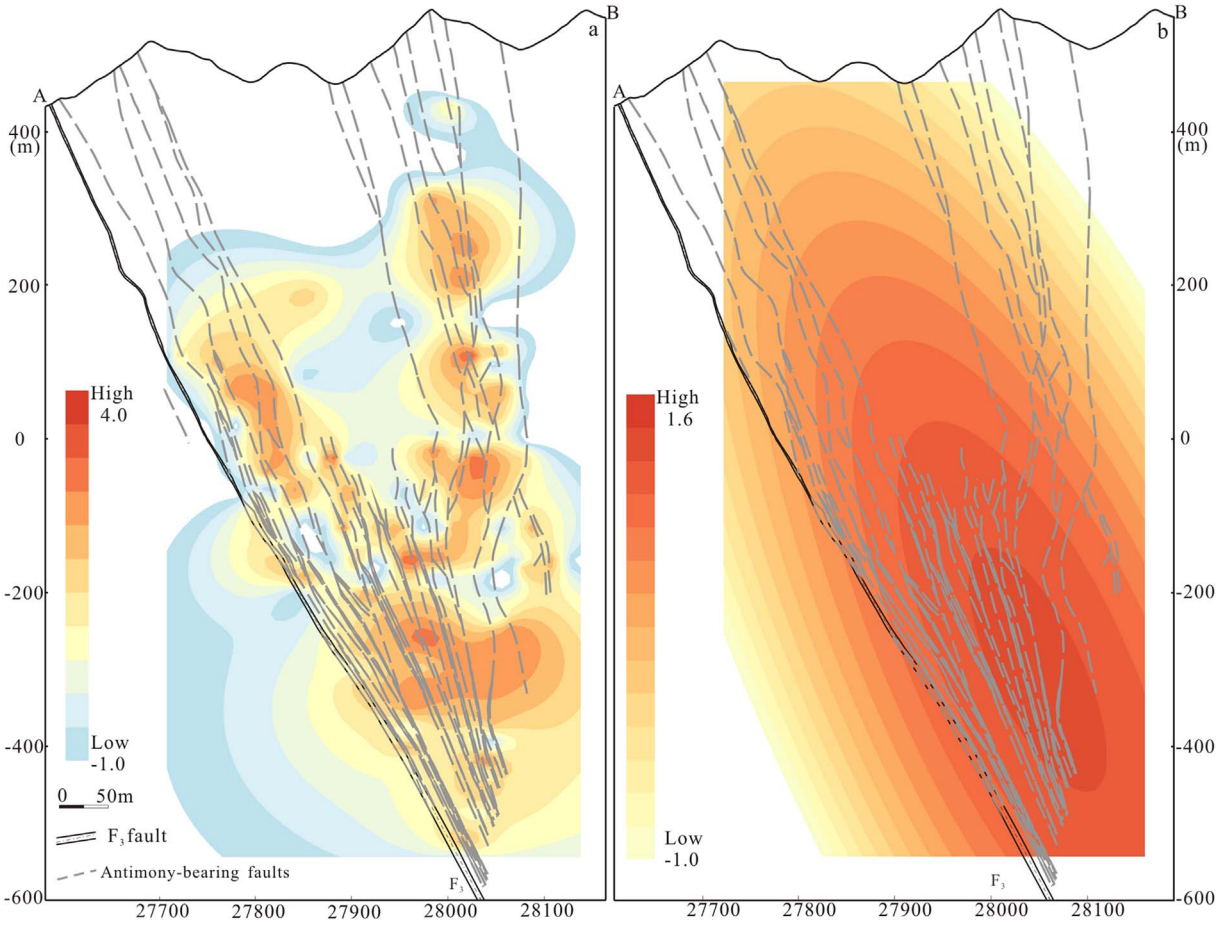

Fig. 13. (a) Sb grade contour map of No.0 cross section in the Zhazixi Sb–W deposit; (b) Quadratic trend surface map of No.0 cross section in the Zhazixi Sb–W deposit.

direction generated the interlayer fractures and successively formed the NW-trending faults in the upper part of the Wuqiangxi Formation. After the orogenic process, the regional kinematic regime transferred to extension, accompanied by a release of compressional stress, and the interlayer fractures and NW-trending faults created a favorable space for Sb and W mineralization.

Both the δD and $\delta^{18}O$ data of the quartz-scheelite and quartz-stibnite veins predominantly plot adjacent to the fields of metamorphic and magmatic fluids. The hydrogen and oxygen isotopic characteristics indicate that the ore-forming fluids were primarily metamorphic or magmatic sources (Fig. 14). However, the lamprophyre dykes are suggested to be negligible to Sb and W mineralization (HBGMR, 2010). Concealed magmatic rocks are absent in the Xuefeng uplift belt according to analysis of gravitational and magnetic anomalies (Liu, 2009). These geological features exclude a contribution from a magmatic source. The $\delta^{34}S_{V\text{-}CDT}$ values (4.7 to 10.4‰) (Bao and Bao, 1991; Bao et al., 1998) are consistent with those of the Proterozoic Wuqiangxi Formation along the Xuefeng uplift belt (Chen, 2012), indicating that the sulfur may be derived from Proterozoic strata. The features of trace element geochemistry in the Xuefeng uplift belt suggest the Meso-Neoproterozoic clastic rocks may be metal sources of Sb and W.

The mineralization of Sb and W may be related to the early Mesozoic intracontinental orogeny. The shallow metamorphic fluids extracted W from the upper part of the Neoproterozoic Wuqiangxi Formation formed a W-bearing fluid and deposited scheelite and quartz in the interlayer fractures. The deeply sourced metamorphic fluids

Table 1
Hydrogen and oxygen isotopic compositions of the Zhazixi Sb–W deposit.

Sample no.	Ore types	Mineral	V-SMOW	V-SMOW	V-SMOW	Th(°C)
			δD_{H2O} (‰)	$\delta^{18}O_{quartz}$ (‰)	$\delta^{18}O_{H2O}$ (‰)	
Z3706	Quartz-scheelite veins	Quartz	−80	16.9	7.89	248.83
Z3255	Quartz-scheelite veins	Quartz	−75	16.4	3.95	188.57
Z3259	Quartz-scheelite veins	Quartz	−66	16.4	3.95	
Z37011	Quartz-stibnite veins	Quartz	−78	17.5	6.86	217.46
Z2503	Quartz-stibnite veins	Quartz	−76	17.8	7.16	
Z1153	Quartz-stibnite veins	Quartz	−90	19	8.36	
Z25013	Quartz-stibnite veins	Quartz	−82	16.2	5.56	
Z25020	Quartz-stibnite veins	Quartz	−88	15.9	5.26	
Z1155	Quartz-stibnite veins	Quartz	−96	15.4	1.84	173.21
Z25014	Quartz-stibnite veins	Quartz	−74	20.3	6.74	

Homogeneous temperatures are examined in the State Key Laboratory of Ore Deposit Geochemistry, Institute of Geochemistry, Chinese Academy of Sciences.

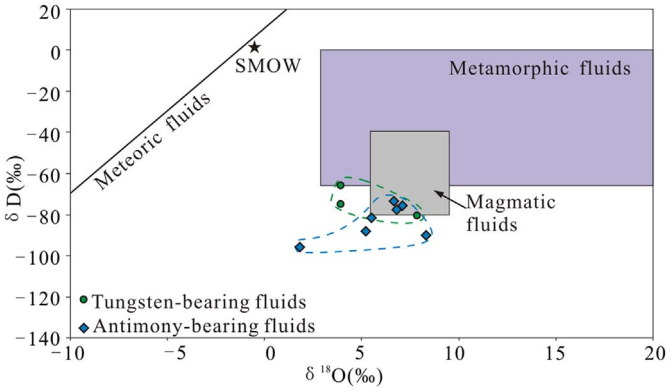

Fig. 14. Plot of δD vs. $\delta^{18}O$ of fluid inclusions in quartz-scheelite and quartz-stibnite veins in the Zhazixi Sb–W deposit. The fields for magmatic and metamorphic water are after Taylor (1979).

extracted Sb from deep Meso-Neoproterozoic clastic rocks. Then the Sb-rich metamorphic fluid migrated from deep to shallow along the F_3 fault and dispersed into the secondary NW-trending faults on the hanging wall through the intersections. Antimoniferous minerals and quartz precipitated gradually, triggered by a fluid mixing or dilution process, which is consistent with the sharp contacts between ore-veins and wallrocks. This metallogenic mechanism has been demonstrated by Williams-Jones and Norman (1997).

6.3. Implications for mineral exploration

Based on the regional structural features and ore grade distribution regularities, the intersections of the secondary NW- and NWW-trending, and the regional NE-trending faults are suggested to be exploring areas for Sb ± W deposits in the Zhazixi Sb ore belt.

The distribution pattern of Sb anomalous ore-shoots implies another unrevealed anomalous ore-shoot at a deep level of the Zhazixi Sb–W deposit. The trend surface of Sb also suggests economic grade Sb mineralization at a deep level. Hence, we suggest that the deep site along the F_3 fault is favorable for Sb exploration.

According to the W distribution regularities, we propose that the interphase distribution of tuffaceous sandstone and thick-bedded sandstone is a favorable sign for W exploration in the Zhazixi Sb–W deposit. The crosscutting relationship between the interlayer fractures and the NW-trending F_3 fault suggests that the W orebodies on the hanging wall may be a shallow part that was displaced and carried to its present position by a sinistrally transpressional tectonic movement of the F_3 fault. Thus, the other, deeper part on the footwall may be located in the southeastern deep site. The horizontal and vertical displacements of the F_3 fault may be a valuable geological indication for future W exploration.

7. Conclusion

The Zhazixi Sb–W deposit is a structurally controlled hydrothermal vein-type deposit with unique element associations of Sb and W. Structures in the Zhazixi Sb–W deposit are dominated by the NW-trending faults and the interlayer fractures. The former are critical to Sb mineralization, which consist of quartz-stibnite veins. In contrast, the latter are closely associated with W mineralization, which are predominantly composed of quartz-scheelite veins. The NW-trending faults experienced a sinistrally transpressional tectonic movement before mineralization, which converted to an extensional kinematic regime during mineralization. The interlayer fractures may form under compressional stress in the NW–SE direction. The Sb and W mineralization may form in two separate metallogenic periods related to the early Mesozoic intracontinental orogeny. Finally, we propose that the deep part of the hanging wall of the F_3 fault may be favorable for Sb exploration, and the deep site on the southeast footwall of the F_3 fault has good potential for W exploration.

Acknowledgements

This research is financially supported by the geological survey project from China Geological Survey (Grant No. 12120113094200) and the Natural Science Foundation of China (Grant No. 41602070). The geologists and miners of the Anhua Zhazixi Antimony Mining Co. Ltd. are thanked for their help during field work. Grateful thanks are also given to Mr. Diwei Luo, Mr. Hang Li, and Mr. Wei Wang for their assistance during laboratory research. We deeply appreciated assistor editor Prof. Jingwen Mao and two anonymous reviewers for their constructive sugggestions and comments, which significantly improved this paper.

References

Akçay, M., 1994. Genesis of the Stibnite–Cinnabar–Scheelite Deposits of the Gümüþler Area, Niðde, Central Turkey and Implications on their Gold Potential. Doctoral Thesis. University of Leicester. http://hdl.handle.net/2381/34995.

Afanas'eva, S.B., Ivanova, G.F., Prokofyev, V.Y., 1994. The Geochemical Characteristics of the Olympiadinskoe Au-(Sb-W) Deposit, Russia // The 9th Symposium of International Association on the Genesis of ore Deposits. Bejing, China, pp. 385–386.

Arribas, A., Gumiel, P., 1984. First occurrence of a strata-bound Sb–W–Hg deposit in the Spanish Hercynian Massif. In: Wauschkuhn, A., Kluth, C., Zimmermann, R.A. (Eds.), Syngenesis and Epigenesis in the Formation of Mineral Deposits, pp. 481–648. http://dx.doi.org/10.1007/978-3-642-70074-3_43.

Bai, D., Jia, B., Zhong, X., Jia, P., Liu, Y., Ma, T., 2011. Neoproterozoic tectonic evolution of the Xuefeng orogenic zone in Hunan. Sediment. Geol. Tethyan Geol. 31 (3), 78–87 (in Chinese with English abstract).

Bao, Z., Bao, Y., 1991. Geologic feature of Zhazixi antimony ore belt and discussion on its ore-forming condition. Hunan. Geol. 10, 25–32 (in Chinese with English abstract).

Bao, Z., Bao, Y., Wang, R., 1998. The geological feature and ore-control factor of stibnite ore belt of Zhazixi and its geological prospection. Beijing Geol. 11–16 (in Chinese with English abstract).

Brogi, A., Fulignati, P., 2012. Tectonic control on hydrothermal circulation and fluid evolution in the Pietratonda–Poggio Peloso (Southern Tuscany, Italy) carbonate-hosted Sb-mineralization. Ore Geol. Rev. 44 (2), 158–171.

Cao, M., Lu, L., 2015. Application of the multivariate canonical trend surface method to the identification of geochemical combination anomalies. J. Geochem. Explor. 153, 1–10.

Chen, G., Yang, X., Liang, X., 2001. Preliminary studies of history-dynamics of the South China mobilized region. Geotecton. Metallog. 25 (3), 228–238 (in Chinese with English abstract).

Chen, A., 2012. Study on Mineralization Regularity and Formation Mechanism of Scheelite and Wolframite in the Woxi Au–Sb–W Deposit in Hunan Province. China University of Geosciences (Beijing), Master Thesis (in Chinese with English abstract).

Clayton, R.N., O'Neil, J.R., Mayeda, T.K., 1972. Oxygen isotope exchange between quartz and water. J. Geophys. Res. 77, 3057–3067.

Dill, H., 1985. Antimoniferous mineralization from the mid-European Saxothuringian zone: Mineralogy, geology, geochemistry and ensialic origin. Geol. Rundsch. 74 (3), 447–466.

Dill, H.G., Weiser, T., Bernhardt, I.R., Kilibarda, C.R., 1995. The composite gold-antimony vein deposit at Kharma (Bolivia). Econ. Geol. 90 (1), 51–66.

Dill, H.G., Pertold, Z., Kilibarda, C.R., 1997. Sediment-hosted and volcanic-hosted Sb vein mineralization in the Potosi region, Central Bolivia. Econ. Geol. 92 (5), 623–632.

Dill, H.G., Melcher, F., Botz, R., 2008. Meso–epithermal W-bearing Sb vein-type deposits in calcareous rocks in western Thailand; with special reference to their metallogenetic position in SE Asia. Ore Geol. Rev. 34 (3), 242–262.

Fan, D., Zhang, T., Ye, J., 2004a. The Xikuangshan Sb deposit hosted by the Upper Devonian black shale series, Hunan, China. Ore Geol. Rev. 24 (1–2), 121–133.

Fan, D., Zhang, T., Ye, J., Pašava, J., Kribek, B., Dobes, P., Varrin, I., Zak, K., 2004b. Geochemistry and origin of tin–polymetallic sulfide deposits hosted by the Devonian black shale series near Dachang, Guangxi, China. Ore Geol. Rev. 24 (1), 103–120.

Gu, X., Schulz, O., Vavtar, F., Liu, J., Zheng, M., Fu, S., 2007. Rare earth element geochemistry of the Woxi W–Sb–Au deposit, Hunan Province, South China. Ore Geol. Rev. 31 (1–4), 319–336.

Gu, X., Zhang, Y., Schulz, O., Vavtar, F., Liu, J., Zheng, M., Zheng, L., 2012. The Woxi W–Sb–Au deposit in Hunan, South China: An example of Late Proterozoic sedimentary exhalative (SEDEX) mineralization. J. Asian Earth Sci. 57, 54–75.

Hagemann, S.G., Lüders, V., 2003. P–T–X conditions of hydrothermal fluids and precipitation mechanism of stibnite-gold mineralization at the Wiluna lode-gold deposits, Western Australia: conventional and infrared microthermometric constraints. Mineral. Deposita 38 (8), 936–952.

He, J., Ma, D., Liu, Y., 1996. Geochemistry of mineralization in the Zhazixi antimony ore belt on the margin of the Jiangnan old land. Mineral Deposits 15 (1), 41–52 (in Chinese with English abstract).

Hinsberg, V.J.V., Zinngrebe, E., Wijs, C.J.D., Vriend, S.P., 2003. A new model for Sb

deposition in the French Massif Central based upon thermodynamic modeling of the mineralizing fluid. J. Geochem. Explor. 78–79 (8), 75–79.
Hu, R., Peng, J., Ma, D., Su, W., Shi, C., Bi, X., Tu, G., 2007. Epoch of large-scale low-temperature mineralizations in southwestern Yangtze massif. Mineral Deposits 26 (6), 583–596 (in Chinese with English abstract).
Hunan Bureau of Geology and Mineral Resources (HBGMR), 1988. Regional Geology of Hunan Province. Geological Publishing House, Beijing, pp. 1–719 (in Chinese).
Hunan Bureau of Geology and Mineral Resources (HBGMR), 2010. Exploration Report of Replaceable Resources in the Zhazixi Sb(W) Ore Deposit, Anhua County, Hunan Province. Unpublished Report. pp. 10–45 (in Chinese).
Li, Z., Li, X., 2007. Formation of the 1300-km-wide intracontinental orogen and post-orogenic magmatic province in Mesozoic South China: a flat-slab subduction model. Geology 35 (2), 179–182.
Li, W., Li, X., Li, Z., Lou, F., 2008. Obduction-type granites within the NE Jiangxi Ophiolite: implications for the final amalgamation between the Yangtze and Cathaysia Blocks. Gondwana Res. 13 (3), 288–301.
Li, X., Li, W., Li, Z., Lo, C., Wang, J., Ye, M., Yang, Y., 2009. Amalgamation between the Yangtze and Cathaysia Blocks in South China: constraints from SHRIMP U–Pb zircon ages, geochemistry and Nd–Hf isotopes of the Shuangxiwu volcanic rocks. Precambrian Res. 174 (1–2), 117–128.
Liang, X., Wei, F., Wang, Y., Hu, B., 1999. On the Mesozoic structural deformation of the Xuefeng Mountain tectonic zone in Hunan. Hunan Geol. 18 (4), 225–228 (in Chinese with English abstract).
Liu, B., 2009. Features and Evolution of Deep Structures in the Xuefeng Intracontinental Tectonic System. Ocean University of China, Master Thesis (in Chinese with English abstract).
Liu, Q., He, L., Huang, F., 2013. Review of Mesozoic geodynamics research of South China. Prog. Geophys. 28 (2), 633–647 (in Chinese with English abstract).
Lu, X., Ma, D., Xie, Q., Wang, W., 2001. Trace element geochemical characteristics of Neoproterozoic-Paleozoic strata in Western and Central Hunan. Geol. Geochem. 29 (2), 24–30 (in Chinese with English abstract).
Ma, D., Pan, J., Xie, Q., He, J., 2002. Ore source of Sb(Au) deposits in Central Hunan: I. Evidences of trace elements and experimental geochemistry. Mineral Deposits 21 (4), 366–376 (in Chinese with English abstract).
Murao, S., Sie, S.H., Hu, X., Suter, G.F., 1999. Contrasting distribution of trace elements between representative antimony deposits in Southern China. Nucl. Instrum. Methods Phys. Res. 150, 502–509.
Neiva, A.M.R., Andráš, P., Ramos, J.M.F., 2008. Antimony quartz and antimony–gold quartz veins from northern Portugal. Ore Geol. Rev. 34 (4), 533–546.
Otofuji, Y.I., Liu, Y., Yokoyam, M., Tamai, M., Yin, J., 1998. Tectonic deformation of the southwestern part of the Yangtze craton inferred from paleomagnetism. Earth Planet. Sci. Lett. 156 (1–2), 47–60.
Peng, B., Chen, G., Piestrzynski, A., 2003. Ore mineralogy of stibnite ore-veins and its genetic implications for the W–Sb–Au ore deposit at Woxi Western Hunan China. Acta Geol. Sin. 23 (1), 82–90 (in Chinese with English abstract).
Peng, B., Frei, R., 2004. Nd–Sr–Pb isotopic constraints on metal and fluid sources in W–Sb–Au mineralization at Woxi and Liaojiaping (Western Hunan, China). Mineral. Deposita 39 (3), 313–327.
Peng, J., Zhang, D., Hu, R., Wu, M., Lin, X., 2008. Sm–Nd and Sr isotope geochemistry of hydrothermal Scheelite from the Zhazixi W–Sb deposit, Western Hunan. Acta Geol. Sin. 82 (11), 1514–1521 (in Chinese with English abstract).
Peng, J., Zhang, D., Hu, R., Wu, M., Liu, X., Qi, L., Yu, Y., 2010. Inhomogeneous distribution of rare earth elements (REEs) in Scheelite from the Zhazixi W–Sb deposit, Western Hunan and its geological implications. Geol. Rev. 56 (6), 810–819 (in Chinese with English abstract).
Qiu, Y., Zhang, Y., Ma, W., 1998. Tectonic and geological evolution of Xuefeng inter-continental orogene, South China. Geolog. J. China Univ. 4 (4), 432–443 (in Chinese with English abstract).
Qiu, Y., Gao, S., Mcnaughton, N.J., Groves, D.I., Ling, W., 2000. First evidence of > 3.2 Ga continental crust in the Yangtze craton of south China and its implications for Archean crustal evolution and Phanerozoic tectonics. Geology 28 (1), 11.
Ren, J., 1990. On the Geotectonic of Southern China. Acta Geol. Sin. (4), 275–288 (in Chinese with English abstract).
Robb, L., 2004. Introduction to Ore-Forming Processes. Blackwell Publishing.
Shu, L., 2006. Predevonian tectonic evolution of South China: from Cathaysian block to Caledonian period folded orogenic belt. Geol. J. China Univ. 12 (4), 418–431 (in Chinese with English abstract).
Shu, L., Yu, J., Jia, D., Wang, B., Shen, W., Zhang, Q., 2008. Early Paleozoic orogenic belt in the eastern segment of South China. Geolog. Bull. China 27, 1081–1093.
Shu, L., 2012. An analysis of principal features of tectonic evolution in South China block. Geolog. Bull. China 31 (7), 1035–1053 (in Chinese with English abstract).
Taylor, H.P., 1979. Oxygen and hydrogen isotope relationships in hydrothermal mineral deposits. In: Barnes, H.L. (Ed.), Geochemistry of Hydrothermal ore Deposits. Wiley, New York, pp. 236–277.
Wagner, T., Cook, N.J., 1998. Sphalerite remobilization during multistage hydrothermal mineralization events—examples from siderite–Pb–Zn–Cu–Sb veins, Rheinisches Schiefergebirge, Germany. Mineral. Petrol. 63, 223–241.
Wagner, T., Cook, N.J., 2000. Late-Variscan antimony mineralisation in the Rheinisches Schiefergebirge, NW Germany: evidence for stibnite precipitation by drastic cooling of high-temperature fluid systems. Mineral. Deposita 35 (2), 206–222.
Wang, Y., Chen, Y., Wang, D., Xu, Y., Chen, Z., 2012. Scheelite Sm–Nd dating of the Zhazixi W–Sb deposit in Hunan and its geological significance. Geol. Chin. 39 (5), 1339–1344 (in Chinese with English abstract).
Wang, C., He, X., Yan, C., Lü, W., Sun, W., 2013. Ore geology, and H, O, S, Pb, Ar isotopic constraints on the genesis of the Lengshuibeigou Pb-Zn-Ag deposit. Chin. Geosci. J. 17 (2), 197–210.
Wang, H., Zuo, R., 2015. A comparative study of trend surface analysis and spectrum-area multifractal model to identify geochemical anomalies. J. Geochem. Explor. 155, 84–90.
Williams-Jones, A.E., Norman, C., 1997. Controls of mineral parageneses in the system Fe–Sb–S–O. Econ. Geol. 92 (3), 308–324.
Wu, J., 1993. Antimony vein deposits of China. Ore Geol. Rev. 8, 213–232.
Wu, R., Zheng, Y., Wu, Y., Zhao, Z., Zhang, S., Liu, X., Wu, F., 2006. Reworking of juvenile crust: Element and isotope evidence from Neoproterozoic granodiorite in South China. Precambrian Res. 146, 179–212.
Yang, S., Blum, N., 1999. Arsenic as an indicator element for gold exploration in the region of the Xiangxi Au–Sb–W deposit, NW Hunan, PR China. J. Geochem. Explor. 66, 441–456.
Yang, Z., Hou, Z., Meng, X., Meng, X., Liu, Y., Fei, H., Tian, S., Li, Z., Gao, W., 2009. Post-collisional Sb and Au mineralization related to the South Tibetan detachment system, Himalayan orogen. Ore Geol. Rev. 36 (1), 194–212.
Yao, J., Shu, L., Santosh, M., 2014. Neoproterozoic arc-trench system and breakup of the South ChinaCraton: Constraints from N-MORB type and arc-related mafic rocks, and anorogenic granite in the Jiangnan orogenic belt. Precambrain Res. 247, 187–207.
Zaw, K., Peters, S.G., Cromie, P., Burrett, C., Hou, Z., 2007. Nature, diversity of deposit types and metallogenic relations of South China. Ore Geol. Rev. 31, 3–47.
Zhai, M., 2013. The main old lands in China and assembly of Chinese unified continent. Chin. Sci. 56 (11), 1829–1852 (Earth Sci. Ed.).
Zhu, Y., Peng, J., 2015. Infrared microthermometric and noble gas isotope study of fluid inclusions in ore minerals at the Woxi orogenic Au–Sb–W deposit, western Hunan, South China. Ore Geol. Rev. 65, 55–69. http://dx.doi.org/10.1016/j.oregeorev.2014.08.014.